$L_{23}[L_{23}]$-$MM[L_{23}]$ and $L_{23}[M^2]$-$MM[M^2]$ Auger vacancy satellite spectra of argon

F. von Busch,[1] U. Kuetgens,[2] J. Doppelfeld,[1] and S. Fritzsche[3]
[1]*Physikalisches Institut, Universität Bonn, Nussallee 12, D-53115 Bonn, Germany*
[2]*Physikalisch-Technische Bundesanstalt, Bundesallee 100, D-38116 Braunschweig, Germany*
[3]*Fachbereich Physik, Universität Kassel, Heinrich-Plett-Strasse 40, D-34132 Kassel, Germany*
(Received 10 July 1998)

The deexcitation of a $1s$ core hole in argon via parallel Auger cascade branches leads to the emission of several superimposed L_{23}-MM vacancy satellite spectra. These spectra arise from the presence of various configurations of additional ''spectator'' holes left by preceding Auger transitions. Such spectator vacancies (henceforth enclosed by brackets) cause characteristic energy shifts and a more complicated multiplet splitting. The most intense lines of the superimposed spectra have been successfully assigned previously. Here we present an extensive refinement and augmentation of that work. The experimental analysis obtained for the two particular L_{23}-MM satellite spectra arising from the principal K-$L_{23}L_{23}$ deexcitation branch is compared to multiconfiguration Dirac-Fock calculations of energies and intensities. Excellent agreement is found, enabling an almost complete assignment of the recognizable lines. Furthermore, by comparison with the electron impact excited L_{23}-MM spectrum a number of other lines are attributed to the normal L_{23}-MM and the $L_{23}[M]$-$MM[M]$ satellite spectrum, which here originate, respectively, from concomitant single primary L_{23} and L_1 ionization. We believe this to be the first comprehensive analysis of a compound Auger cascade spectrum. [S1050-2947(99)06803-1]

PACS number(s): 32.30.−r, 32.80.Hd, 31.15.Ar

I. INTRODUCTION

Auger spectroscopy usually deals with spectra arising from the relaxation of a single core hole. Prime examples are the spectra of rare gases observed after ionization at the uppermost inner shell [1–3]. In such spectra, however, there always appear also lines originating from the decay of two-hole initial states, because the primary ionization processes create, along with single core vacancies, at a minor rate also double holes. An additional hole, while basically being only a spectator to the Auger process, changes the screening. Thereby it causes a characteristic shift of the transition energy and thus gives rise to a so-called vacancy satellite line. Moreover, it modifies the angular momentum coupling so that the satellite spectrum is not merely a shifted image of the normal one. The high-resolution L_{23}-MM spectrum of argon, for example, exhibits numerous weaker lines that have been classified as belonging to $L_{23}M$-MMM transitions [1,3], i.e., as vacancy satellites derived from an M spectator hole. Up to now, even this common example of a vacancy satellite spectrum has in large part not been analyzed successfully. The reason is the presence of several open shells in the initial as well as the final states, which leads to a rather congested spectrum and makes accurate calculations an arduous task.

Both of these difficulties increase with the number of open shells. Multiple-vacancy Auger spectra have been frequently observed in heavy-particle collisions, where they arise from primary multiple ionization or from Auger cascades. A detailed analysis usually is hampered already by an insufficient knowledge of the initial-state distribution. However, such spectra can be excited in a much better-defined and at the same time very efficient way by deep-core single photoionization. In this case, multiple vacancies are generated in the course of the deexcitation, and their distribution therefore is rather independent of the primary ionization process. All of the second and later transitions of the decay cascade occur in the presence of additional holes left by the preceding steps. Hence the vacancy ''satellites'' (or hypersatellites, as they are called if the spectator hole is located at an inner shell) are not merely weak accessories, but are the main lines of the cascade spectrum and altogether carry the full spectral intensity.

Photoexcitation at energies above the $1s$ ionization threshold therefore has been employed by von Busch *et al.* [4] in order to investigate the L_{23}-MM cascade spectrum of argon. However, even this comparatively simple example of a second-step Auger spectrum is complicated by the fact that the various branches of the deexcitation cascade give rise to several coexisting and superimposed spectra, which originate from basically similar transitions and are distinguished from each other only by the presence of different configurations of spectator holes. For the L_{23}-MM spectra of argon emitted after K, L_1, or L_{23} ionization this is schematically depicted in Fig. 1. Such spectra fall into roughly the same energy interval and are very rich in lines due to the open-shell structure of the ions. Their superposition therefore will be extremely complex and difficult to investigate. Apart from cases where one of the overlapping spectra (or part of it) clearly dominates over the others one has to resort to coincidence methods [6] in order to disentangle specific transitions to be studied.

For example, the overlapping spectra emitted on parallel branches of the deexcitation cascade lead to different final ionic charges (Fig. 1). Thus electron spectroscopy performed in coincidence with a charge analysis of the resulting ions made it possible to fully decompose the L_{23}-MM spectrum of argon emitted after photoionization above the $1s$ threshold

 ©1999 The American Physical Society

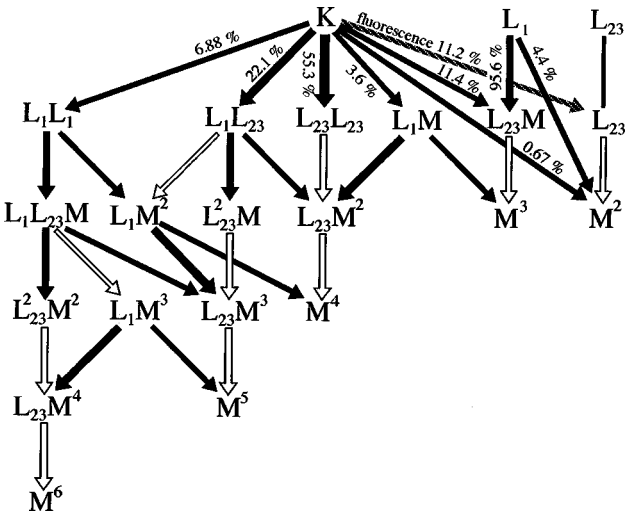

FIG. 1. Schematic representation of the vacancy configurations and the transitions arising in the deexcitation of primary K, L_1, and L_{23} holes. White arrows signify the various L_{23}-MM vacancy satellite transitions. Shake transitions are omitted for the sake of clarity. The indicated branching ratios have been taken from [5].

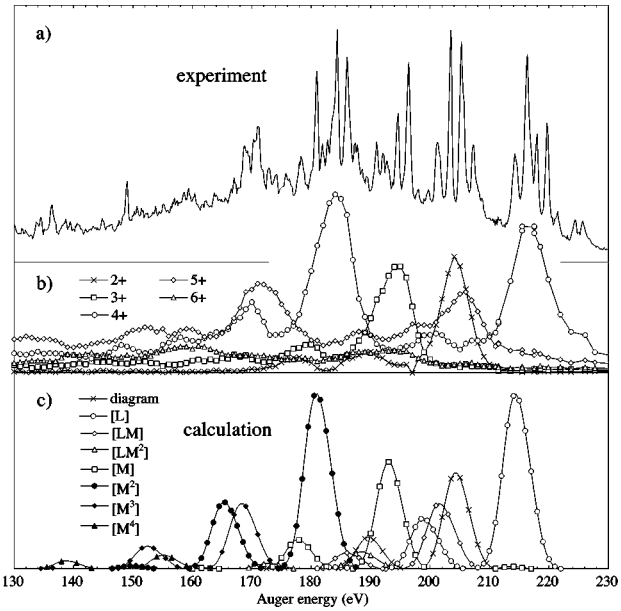

FIG. 2. (a) L_{23}-MM Auger spectrum observed after broadband photoexcitation mainly above the 1s threshold [4]; (b) spectral distribution of L_{23}-MM electrons observed in coincidence with final ions of charges 2–6 [7] and (c) transition multiplets of the partial L_{23}-MM spectra, emitted in the presence of various spectator vacancy configurations as indicated (bar spectrum calculated in single configuration average [4], convolved with a Gaussian of 4 eV FWHM in order to mimick the multiplet splitting).

[Fig. 2(a)] into the partial vacancy satellite and hypersatellite spectra [Fig. 2(b)] [7]. The results are in very good agreement with those of a step-by-step calculation of the cascade in single configuration average approximation [Fig. 2(c)] [4,8]. Further confirmation has come from electron-electron coincidence spectroscopy, by which the sequential relationship of certain partial spectra (Fig. 1) has been studied [7].

However, neither the calculation nor the coincidence experiments address individual spectral lines, because the former ignores the multiplet splitting and the latter have been performed at low energy resolution ($\Delta E = 5$ eV). Thus the assignment of lines to a partial spectrum is fairly obvious only when they are intense and happen to fall into an energy interval that has been shown to be dominated by transitions belonging to just one specific configuration of spectator vacancies. Prime candidates are here the L_{23}-$M_{23}M_{23}$ multiplets, which represent the strongest lines of a partial spectrum, and especially those of the spectra lying in the most intense branch of the deexcitation cascade. The results of the aforementioned calculation [4] and the electron-ion coincidence measurements [7] demonstrate that indeed the condition is met by the ''normal'' L_{23}-$M_{23}M_{23}$ multiplet (without spectator holes) as well as by the $L_{23}[M]$-$M_{23}M_{23}[M]$, $L_{23}[L_{23}]$-$M_{23}M_{23}[L_{23}]$, and $L_{23}[M_{23}^2]$-$M_{23}M_{23}[M_{23}^2]$ ones. These correspond largely to the groups of prominent lines around 205, 195, 216, and 184 eV, respectively (Fig. 2). (Here and in the following we denote the various partial L_{23}-MM spectra by the configuration of spectator holes set in square brackets, e.g., $L_{23}[M^2]$-$MM[M^2]$ or simply $[M^2]$.) Starting from this gross assignment, an analysis of the resolved lines belonging to the $[L_{23}]$ and $[M_{23}^2]$ spectra has been given by von Busch *et al.* [4].

The purpose of the present work is twofold: to extend and refine the previous experimental analysis [4,9], and to compare the results with a relativistic multiconfiguration calculation of transition energies and intensities. Details of the experiment and of the calculation will be given, respectively, in Secs. II and III of the paper. Section IV presents the results. Here we identify in Sec. IV A observed lines that are emitted following a single primary L_{23} or L_1 ionization (which always accompany K ionization) or certain equivalent K hole deexcitation steps, such as, e.g., a radiative K-L_{23} transition. These lines belong to the ''normal'' L_{23}-MM or the $L_{23}[M]$-$MM[M]$ satellite spectrum and are known from the electron impact excited L_{23}-MM spectrum, which has been rather thoroughly investigated in the past [1,3,10,11]. Section IV B gives the experimental analysis of those transitions that arise from the strongest branch of K hole deexcitation and are the principal subject of this article. The results are compared in Sec. IV C with multiconfiguration Dirac-Fock (MCDF) calculations, which will be shown to confirm them and moreover to enable an extension of the assignments to almost all other discernible and as yet unidentified lines. A summary concludes the paper.

II. EXPERIMENT

The experimental setup utilized in taking the Auger spectra is the same as that used by von Busch *et al.* and has been described before [4,7]. The measurements were performed at the electron accelerator ELSA at Bonn which was operated at 2.3 GeV electron energy in storage mode. The ''white'' x-ray beam from a bending magnet was filtered by a 125-μm Be window. This leaves an excitation spectrum extending between 1.5 and approximately 10 keV, from which primary single photoionization at the K, L_1, and L_{23} shells of argon has been calculated to occur in approximate proportions of 1 : 0.24 : 0.18. The target density of argon gas, which effuses from a hypodermic needle, is estimated to be

around 3×10^{13} atoms/cm^3, whereas the total light flux is equivalent to roughly 2×10^{12} effective photons/s at the K edge.

The spectra were taken with a rotationally symmetric electron spectrometer (MAC 2, Riber) resembling in geometry a double-pass cylindrical mirror analyzer but employing retardation. This instrument was oriented perpendicularly to the accelerator plane and operated at 0.35 eV energy resolution. Spectra were recorded stepping the energy by 0.05 eV increments in repeated scans at 500 ms dwell time per data point. The spectra have been calibrated [7] against the electron impact excited highly resolved L-MM spectrum of argon published by Werme, Bergmark, and Siegbahn [3]. This is possible because a number of lines from this spectrum can be recognized also in the broadband photoexcited one. The uncertainty of calibration (relative to that of the spectrum measured by Werme, Bergmark, and Siegbahn) is estimated to be 0.064 eV.

III. CALCULATIONS

The creation and decay of inner-shell vacancy states are often efficiently described by a two-step model [12]. In such a model, one assumes intermediate atomic states that are prepared rather independent of the creation process. They are usually referred to as the initial states of a given Auger spectrum. The decay of these excited states then leads to a set of final ionic states, which in a cascade may again become the initial ones of a subsequent Auger transition.

Initial and final bound states of autoionizing argon ions, which arise in the deexcitation of a $1s$ vacancy state, have been calculated in the framework of the MCDF model [13]. In this approximation, the atomic wave functions are built up from a linear combination of configuration state functions (CSF's). By means of such a superposition all strong configuration interactions among nearly degenerate atomic levels can be taken into account. A representation of the atomic states in the adopted CSF basis, i.e., the mixing coefficients, is then obtained by diagonalizing the corresponding Hamiltonian matrix.

In order to generate the atomic bound states we used the relativistic structure code GRASP^2 [14,15] which we extended for the calculation of Auger transition probabilities. In GRASP^2 the radial orbitals are generated self-consistently with respect to the Dirac-Coulomb Hamiltonian. The relativistic (transverse) Breit interactions are added later to the Hamiltonian matrix as a perturbation, but these contributions are of lesser importance for light elements like argon.

New modules for the GRASP code have been developed during recent years for numerical integration of the continuum orbitals as well as for the calculation of transition amplitudes and scattering phases [15,16]. This program for relativistic Auger transition rates (RATR) has been employed in the present work for the calculation of transition energies and relative intensities. Here we will give only a brief account of the underlying theory; a more detailed description of the program RATR has been presented elsewhere [17,18].

In RATR, the single-particle continuum functions of the outgoing electrons are generated in the local jj-averaged potential of the final ionic states. For the present case, we neglect the exchange with the bound electrons because typical transition energies are a few hundred electron volts. A WKB method similar to the one employed by Ong and Russek [19] is used to obtain the normalization and phases of the continuum orbitals. Before normalization, however, these orbitals of the emitted electrons are orthogonalized with respect to all orbitals of the corresponding initial state multiplet because it is with this set of orbitals that all Auger amplitudes are calculated. Thus, relaxation of the orbital functions due to the Auger emission is not taken into account. Moreover, only the dominant Coulomb repulsion is considered in the computation of the transition matrix.

Our calculations describe the atomic states in intermediate coupling. Even though we shall often refer to additional vacancies as ''spectators'' we included all dominant configuration interactions for the calculation of energies as well as Auger rates. In particular, the important intrashell interactions between the core electrons and the spectator holes have been fully taken into account.

The L_{23}^{-2} vacancy states in the $L_{23}[L_{23}]$-$MM[L_{23}]$ satellite spectrum have a closed-shell valence structure and hence are properly described by including the corresponding configuration states with just two L holes. In contrast, the final $L_{23}^{-1}M^{-2}$ multiplet of this spectrum shows a much more complex fine structure. The coupling of the single $2p$ hole with the electrons from the $3s$ and/or $3p$ subshells results in 18 CSF's with even parity and 23 CSF's with odd parity. Total angular momenta J of the corresponding atomic levels range from 1/2 to 7/2. The subsequent $L_{23}[MM]$-$MM[MM]$ transitions in turn lead to a final M^{-4} multiplet comprising 10 CSF's of even and 10 of odd parity. For both the $L_{23}^{-1}M^{-2}$ and the M^{-4} multiplets, sufficiently accurate splittings and transition energies cannot be obtained when only the aforementioned small CSF basis is used in the expansion of the wave functions. Instead, for many of the states a considerably more refined description is required. The inclusion of additional virtually excited configurations will, however, rapidly lead to computational problems. In order to keep the calculations feasible we therefore performed them subject to various restrictions, either with respect to the number of configurations considered or to the range of final J values, and compared the results to make sure that they are mutually consistent to a sufficient degree.

Before starting with energy calculations we note that the splittings of the upper $2p^4$ levels of the $L_{23}[L_{23}]$-$MM[L_{23}]$ spectrum have been measured [20], while those of the lower ones must be supplied by theory. Most final levels of the subsequent $L_{23}[M^2]$-$MM[M^2]$ transitions in turn are known from optical spectroscopy [21]. Thus only a few of these, in particular, the $3s^03p^4$ ones, need to be determined by calculation.

Energies of the 21 intermediate $2p^53s^23p^4$ levels have been calculated for $J=1/2,\ldots,7/2$ including all configurations $2p^53s^h3p^k3d^l$ with hkl = 240, 222, 141, and 060 (in total 878 CSF's). The results for this multiplet, which of all those investigated here can be compared best to observation, have been obtained using the EOL (extended optimized level) approximation [22]. AL (average level) calculations, while for most levels giving good agreement with experiment, produced for some specific ones deviations of up to 0.5 eV from the observed splittings, which persisted when higher virtual excitations were included. All the remainder of

TABLE I. Calculated $2p^5(3s^23p^4+3s^13p^5+3s^03p^6)(=LM^2/n)$ levels of Ar^{3+}, enumerated by $n=1,\ldots,41$. Π,J,E, and ΔE denote, respectively, the parity, total angular momentum, energy, and width ($a[-n]$ stands for $a\times10^{-n}$). The remaining columns give the weights of configurations $2p^53s^h3p^k3d^l$, with numbers in italics indicating hkl. See text for details.

n	Configur.	Π	J	E (eV)	ΔE (eV)	*240*	n	Configur.	Π	J	E (eV)	ΔE (eV)	*150*	*231*
1	$2p^53s^23p^4$	–	1/2	322.64	8.33[-3]	0.958	22	$2p^53s^13p^5$	+	7/2	337.89	3.84[-3]	0.736	0.228
2		–	7/2	323.17	6.29[-3]	0.956	23		+	5/2	338.53	2.24[-2]	0.730	0.233
3		–	5/2	323.64	6.92[-3]	0.955	24		+	3/2	338.59	2.06[-2]	0.731	0.234
4		–	5/2	323.91	5.91[-3]	0.955	25		+	1/2	338.63	2.48[-2]	0.732	0.233
5		–	3/2	324.11	1.19[-2]	0.955	26		+	3/2	339.11	4.35[-2]	0.722	0.240
6		–	3/2	324.43	1.55[-2]	0.955	27		+	5/2	339.85	1.80[-1]	0.690	0.274
7		–	1/2	324.57	9.39[-3]	0.955	28		+	3/2	339.90	6.02[-2]	0.716	0.247
8		–	3/2	325.21	6.42[-2]	0.954	29		+	1/2	340.41	5.22[-2]	0.722	0.243
9		–	5/2	325.46	1.00[-2]	0.955	30		+	1/2	340.76	1.37[-1]	0.690	0.273
10		–	1/2	325.84	3.82[-3]	0.955	31		+	3/2	341.32	1.06[-1]	0.694	0.269
11		–	1/2	326.12	4.42[-3]	0.954	32		+	3/2	342.05	1.05[-1]	0.696	0.266
12		–	7/2	326.14	6.51[-3]	0.952	33		+	5/2	342.29	6.17[-2]	0.653	0.311
13		–	3/2	326.27	8.90[-2]	0.953	34		+	1/2	343.51	6.12[-2]	0.624	0.339
14		–	3/2	327.04	2.28[-1]	0.952	35		+	5/2	344.23	1.13[-1]	0.527	0.440
15		–	5/2	327.85	3.95[-2]	0.953	36		+	3/2	344.36	1.17[-1]	0.350	0.617
16		–	3/2	328.75	2.63[-1]	0.947	37		+	1/2	345.02	1.28[-1]	0.592	0.374
17		–	5/2	329.43	2.84[-1]	0.952	38		+	3/2	346.17	3.41[-2]	0.305	0.662
18		–	1/2	329.75	1.76[-1]	0.948	39		+	1/2	346.88	8.08[-2]	0.201	0.762
19		–	3/2	329.55	5.76[-2]	0.926							*060*	*141*
20		–	3/2	331.15	3.18[-1]	0.949	40	$2p^53s^03p^6$	–	3/2	359.38	9.12[-2]	0.409	0.474
21		–	1/2	331.61	1.50[-1]	0.919	41		–	1/2	361.60	8.77[-2]	0.400	0.478

our computations have been performed in the AL mode [22].

For calculation of the $2p^53s^13p^5$ levels we expanded the wave function into the configurations $2p^53s^h3p^k3d^l$ with hkl = 150, 132, 051, 231, and 213. Separate computations have been run, respectively, for $J=5/2$ and 7/2 (1039 CSF's), $J=3/2$ and 5/2 (1071 CSF's), and $J=1/2$ and 5/2 (867 CSF's), and the resulting energies have been matched to each other for the $J=5/2$ levels. The distance of the $2p^53s^13p^5$ levels to the $2p^53s^23p^4$ ones was determined from an independent calculation for $J=5/2$, which included the configurations hkl = 240, 222, 141, 150, 132, 051, 231, and 213 (783 CSF's). Finally, we calculated the splitting of the two $2p^53s^03p^6$ levels and obtained their position relative to the $2p^53s^23p^4$ ones from a run with hkl = 240, 222, 141, 060, and 042, and $J=3/2$ (339 CSF's). From our experience we estimate the effect of neglected configurations upon the splittings to be below ±0.2 eV.

Turning then to the final Ar^{4+} levels of the subsequent $L_{23}[M^2]$-$MM[M^2]$ transitions, we obtained the $3s^03p^4$ ones relative to the spectroscopically measured $3s^23p^2$ and $3s^13p^3$ levels from a calculation based on the configurations $3s^h3p^k3d^l$ with hkl = 220, 202, 040, 022, 121, and 103, and $J=0$, 1, 2 (127 CSF's). Similarly, the unknown $^5S_2$ level has been located within the $3s^13p^3$ multiplet by a calculation including hkl = 130, 112, 031, and 211, and $J=0,\ldots,3$ (120 CSF's). This completes the determination of the required multiplet splittings. The absolute energy separations between the Ar^{2+}, Ar^{3+}, and Ar^{4+} multiplets have been determined by shifting the entire groups so as to bring the calculated transition energies into agreement with the observed spectrum, as will be detailed in Sec. IV C. The quoted absolute energies of all levels thus are referred to the experimental value of the $2p^4(^1D_2)$ energy.

Henceforth we shall call the 21 levels with the greatest weight of the $2p^53s^23p^4$ configuration ''the $2p^53s^23p^4$ levels'' and enumerate them by LM^2/n, $n=1,\ldots,21$. Similarly we denote by LM^2/n with $n=22,\ldots,39$ the 18 levels of largest $2p^53s^13p^5$ content, and with $n=40$, 41 the two $2p^53s^03p^6$ levels (cf. Table I). The numbering is in sequence of ascending energy *as calculated with the following more restricted configuration basis*: hkl=240, 060 for k=1,...,21, hkl=150 231 for $k=22,\ldots,39$, and hkl= 060 141 for k=40, 41. This sequence has been chosen because it is well defined, although in some places it may deviate from the order found with a larger expansion, which for some levels depends quite critically on the particular choice of basis. Likewise we enumerate the final Ar^{4+} levels by M^4/n with $n=1,\ldots,5$ for the nominal $3s^23p^2$ ones, $n=6,\ldots,15$ for $3s^13p^3$, and $n=16,\ldots,20$ for $3s^03p^4$ (cf. Table II).

For the calculation of *line intensities* slightly less accurate wave functions were deemed sufficient. With respect to transitions $2p^4(^1D_2,^1S_0)\rightarrow2p^5(3s^23p^4+3s^13p^5+3s^03p^6)$ the expansion for the lower levels comprised the configurations $2p^53s^h3p^k3d^l$ with hkl = 240, 150, 060, 141, and 231, and $J=1/2,\ldots,7/2$ (474 CSF's). Calculating Auger rates of the subsequent transitions, which lead to $(3s^23p^2+3s^13p^3+3s^03p^4)$, we included the same configurations for the upper levels, whereas the lower ones were expanded into $3s^h3p^k3d^l$ with hkl = 220, 130, 040, 211, and 121, and $J=0,\ldots,3$ (65 CSF's). Virtual excitation to the $3d$ shell contributes quite markedly to the description of all states with an open $3s$ shell (cf. Tables I and II). Such virtually excited configurations have vanishing Auger matrix elements with

TABLE II. Calculated $3s^2 3p^2 + 3s^1 3p^3 + 3s^0 3p^4 (= M^4/n)$ levels of Ar^{4+}, enumerated by $n = 1, \ldots, 20$. Π, Q, and E denote, respectively, the parity, quantum symbol and energy. The remaining columns give the weights of configurations $3s^h 3p^k 3d^l$, with numbers in italics indicating hkl. Unless indicated otherwise, energies are spectroscopic values [21] referred to the Ar^{4+} ground level at 143.04 $\pm$ 0.33 eV.

n	Configur.	Π	Q	E (eV)	*220*		n	Configur.	Π	Q	E (eV)	*130*	*211*
1	$3s^2 3p^2$	+	$^3P_0$	143.04	0.952		6	$3s^1 3p^3$	–	$^5S_2$	153.19[a]	0.988	0.000
2		+	$^3P_1$	143.15	0.952		7		–	$^3D_1$	158.12	0.840	0.136
3		+	$^3P_2$	143.29	0.952		8		–	$^3D_2$	158.13	0.841	0.136
4		+	$^1D_2$	145.06	0.952		9		–	$^3D_3$	158.14	0.842	0.135
5		+	$^1S_0$	147.74	0.933		10		–	$^3P_2$	160.62	0.830	0.142
n	Configur.	Π	Q	E (eV)	*040*	*121*	11		–	$^3P_1$	160.62	0.833	0.139
16	$3s^0 3p^4$	+	$^3P_2$	175.79[a]	0.481	0.497	12		–	$^3P_0$	160.62	0.834	0.139
17		+	$^3P_1$	175.93[a]	0.477	0.501	13		–	$^1D_2$	162.16	0.457	0.502
18		+	$^3P_0$	176.00[a]	0.476	0.502	14		–	$^3S_1$	166.79	0.936	0.054
19		+	$^1D_2$	176.88[a]	0.576	0.376	15		–	$^1P_1$	167.26	0.822	0.146
20		+	$^1S_0$	182.33[a]	0.510	0.391							

[a]Calculated, see text.

the respective leading configurations of the combining levels. In some cases this leads to a considerable reduction of the transition rate. All intensity calculations have been performed in the AL mode.

It should be noted that a treatment of the decay probabilities similarly elaborate as carried out for the transition energies would require to incorporate also the multichannel scattering character of the Auger emission, and thus properly would have to go beyond a merely increased extent of virtual excitations in the expansion of the wave function. However, experimental intensities to compare with can be determined from the present spectrum only somewhat crudely, due to the strong background originating from other transitions. The calculated intensities are certainly accurate enough to remove any ambiguities in matching the experimental and theoretical spectra. Indeed they are quite close to the observed ones, as will be seen.

Extensive trial calculations have been run with varying success, depending markedly on the computer system being used. Calculations on the optimized level (OL) and extended optimized level (EOL) levels in general could not be brought uniformly to convergence. The final calculations were performed on a 150-MHz PC type computer with 16 MB RAM and processor AMD-K5-PR150, running under Microsoft Windows95® with compiler FORTRAN PowerStation 4.0®. Typical computing times were on the order of several hours per run. Complete listings of energies and transition probabilities are available upon request from one of us (U.K.). Results of our calculations will be presented and compared to experiment in Sec. IV C.

IV. RESULTS

A. L_{23}-MM diagram and [M] vacancy satellite lines

The L_{23}-MM spectrum excited by broadband hard x-rays has been measured over the energy range between 170 and 230 eV at a resolution of 0.35 eV. We have also taken the Auger spectrum excited by 3 keV electrons between 145 and 220 eV. Apart from having lower resolution this spectrum shows no significant differences to the one published by Werme, Bergmark, and Siegbahn [3]. Virtually all of the known L_{23}-MM transitions without a spectator vacancy that can be recognized in our spectrum (numbers 32, 37, 45, 48, 52, 60, 72, 73 + 74, 75, 76, and 78 in the count of Werme, Bergmark, and Siegbahn) are found also in the photoexcited spectrum, as is evident from the comparison of both spectra given in Fig. 3. A linear regression to almost all of them has been used to calibrate the photoexcited spectrum. For assignments of these lines the reader is referred to the work of Werme, Bergmark, and Siegbahn [3], McGuire [10], Dyall and Larkins [11], and Hansen and Persson [23].

There is a striking similarity between both experimental spectra with respect to the group of lines around 205 eV. In the electron impact excited spectrum this group is made up by the strong L_{23}-$M_{23}M_{23}$ diagram lines, but in the photoexcited spectrum it obviously contains additional transitions. These have been located at 199.7, 201.5, 206.1, and about 207.9 eV. From the electron-ion coincidences it follows that they most likely are $L_{23}[L_{23}]$-$M_1 M_{23}[L_{23}]$ or $L_{23}[L_{23}M]$-$M_{23}M_{23}[L_{23}M]$ lines (Fig. 2). Actually the calculations to be reported below identify those observed at 199.7 and 201.5 eV as due to $2p^4(^1D_2) \rightarrow 2p^5 3s^1 3p^5$ transitions (Fig. 4), whereas the additional intensity around 206 and 208 eV must be attributed mostly to $2p^4 3s^2 3p^5 \rightarrow 2p^5 3s^2 3p^3$ transitions, in accordance with the maximum observed in the e-Ar^{5+} coincidence distribution around these energies (Fig. 2). The initial $L^{-2}M^{-1}$ levels of the $L_{23}[LM]$-$M_{23}M_{23}[LM]$ spectrum are very numerous and are, according to an MCDF calculation [20], spread over 44.6 eV. Therefore the $[LM]$ spectral intensity is distributed over a broad energy range, as is shown also by the e-Ar^{5+} coincidence data [Fig. 2(b)]. This is the origin of a large part of the quasicontinuous background between 190 and 210 eV.

The photoexcited spectrum has other lines in common with the electron impact excited one, which have been identified as belonging to the [M] spectator vacancy spectrum (Fig. 3). This spectrum arises partly from primary L_1 holes turned into $L_{23}M$ double vacancies by a Coster-Kronig transition (whence it is called the ''transfer spectrum'' by Coo-

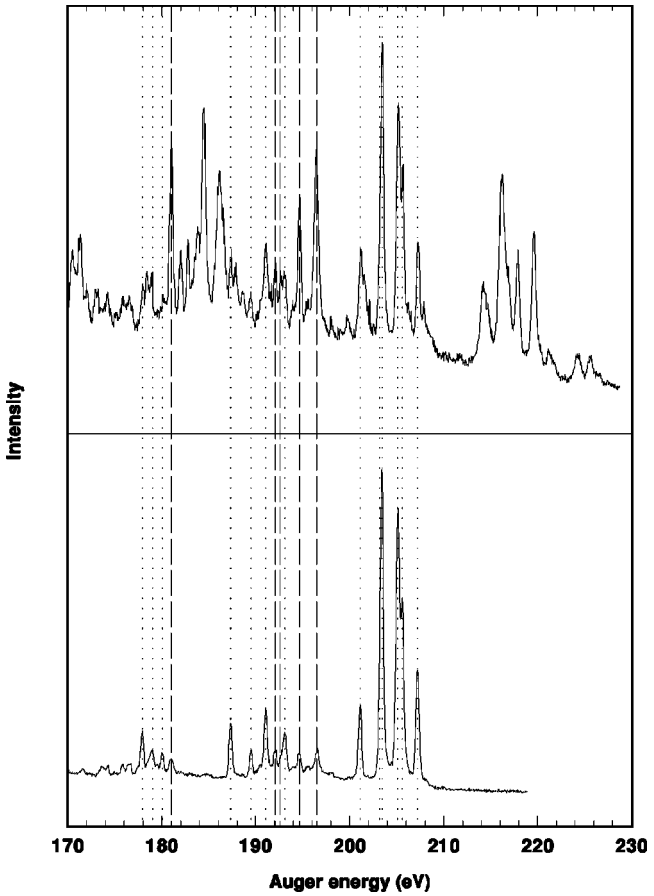

FIG. 3. L_{23}-MM Auger spectrum of argon as observed after broadband photoexcitation mainly at energies above the K edge (top), and as excited by impact of electrons with 3 keV (bottom). Dotted and dashed lines indicate transitions common to both spectra and belonging, respectively, to the L_{23}-MM and the $L_{23}M$-MMM partial spectra.

per *et al.* [24]), partly via K ionization and a subsequent K-$L_{23}M$ transition and, to a lesser extent, also via direct $L_{23}M$ double ionization. The pertinent lines are all much stronger than in the electron impact excited spectrum though not all in the same proportion. While the ones at 192.1 and 192.6 eV are roughly doubled in intensity compared to electron impact excitation, those at 194.7 and 196.5 eV have grown sevenfold. On the other hand, it can be seen in the spectra taken by Cooper *et al.* [24] after photoexcitation *below* the K edge that these latter two lines grow only proportionately to the other $L_{23}[M]$-$MM[M]$ lines as the photon energy and thereby the fraction of primary L_1 holes is increased. This shows that with photoexcitation *above* the $1s$ threshold the initial states of the lines at 194.7 and 196.5 eV are preferentially populated by K ionization and a subsequent K-$L_{23}M$ Auger step. Asplund *et al.* [20] have measured the K-LM spectrum and found that about half of the K-$L_{23}M$ intensity is contained in a line of 1.46 eV width at 2923.35 eV, which they attribute to closely lying $2p^5 3p^5(^1D_2 + {}^3S)$ levels. Of these two levels, the $^1D_2$ one (labeled 2a in intermediate coupling by McGuire [10]) is expected to give the larger contribution. If we tentatively identify this level as the common initial one of the lines at 194.7 and 196.5 eV, then with the aid of known $3p^3$ levels and transition probabilities calculated by McGuire [10] the final states of these lines can be identified, respectively, as $3p^3(^2P)$ and $3p^3(^2D)$, in accordance with the assignment given by Werme *et al.* to lines 64 (194.66 eV) and 67 (196.42 eV) observed in the electron impact excited L_{23}-MM spectrum [3]. From the same data a third line of comparable intensity, leading from the $2p^5 3p^5(^1D_2)$ to the $3s^1 3p^4(^2D)$ level, is expected at 181.0 eV where it coincides with one of the strong $[M^2]$ vacancy satellites to be discussed below. Line 68 observed at 196.67 eV by Werme, Bergmark, and Siegbahn and tentatively assigned by them as $L_{23}M_{23}(^1S_0) \rightarrow M_{23}^3(^2P)$ seems to be less populated via K ionization.

Cooper *et al.* [24] have modelled the $[M]$ spectrum on the basis of published initial and final level energies and transition probabilities. Although the result, when superimposed in suitable proportion with the normal L_{23}-MM spectrum, resembles the spectrum measured by them after photoexcitation at 3174 eV (still below the K threshold), the line spacing is not fully resolved, and the agreement of calculated and observed relative intensities is only fair. Actually the number of possible transitions is so large that the authors were not able to assign individual lines. In the present case the difficulties are aggravated by the superposition with other partial spectra (cf. Fig. 2). Our own attempts to assign the $[M]$ satellites, identified in Fig. 3, with the aid of published data on level energies and transition probabilities [10,20] also ended up in ambiguities.

B. $[L_{23}]$ and $[M^2]$ vacancy satellite lines: Experimental analysis

The most important deexcitation branch following K ionization is the one leading via a K-$L_{23}L_{23}$ transition and sequential emission of $[L_{23}]$ and $[M^2]$ vacancy satellites to final Ar^{4+} ions (Fig. 1). As can be seen in Fig. 2 the L_{23}-$M_{23}M_{23}$ groups belonging to the respective partial spectra by far dominate the spectral intensity in the pertinent energy intervals. Hence we may tentatively attribute the strongest individual lines accordingly. Another favorable circumstance, which allows us to confirm such assignments, is that the initial levels of the $[L_{23}]$ and the final ones of the $[M_{23}^2]$ satellites are few in number and their energies are known. Thus one can search for pairs of lines—with one line around 216 eV and the other one around 184 eV—whose sum of transition energies corresponds to one of the $2p^4$- $3p^2$ term differences [4]. Such a pair identifies the respective lines as being emitted in cascade and locates an intermediate $2p^5 3p^4$ level.

Line positions in the intervals 175 to 190 eV and 210 to 230 eV of our photoexcited spectrum have been determined, after subtraction of an estimated background, by fitting Gaussians of 0.45 eV full width at half-maximum (FWHM) to individual spectral maxima. In some cases the observed lines are so broad that two Gaussians have been assumed. Transition energies determined in this way are given, respectively, in Tables III and IV for the lines assigned to the $[L_{23}]$ and the $[M^2]$ spectrum. Entries in parentheses refer to overlapped lines and are likely to depend somewhat on the conditions imposed on the fit.

By far the majority (87%) of initial K-$L_{23}L_{23}$ transitions ends up in the $2p^4(^1D_2)$ level [20]. Combining the $1s$ ionization potential of 3206.26(30) eV [25] with the Auger en-

TABLE III. Transitions $2p^4 \rightarrow 2p^5(3s^2 3p^4 + 3s^1 3p^5 + 3s^0 3p^6)$. Lower levels are enumerated as LM^2/n, $n = 1, \ldots, 41$ (Table I). J is the total angular momentum, I the intensity, ΔE the linewidth. The total intensity of the transitions $2p^4(^1D_2) \rightarrow 2p^5 3s^2 3p^4$ has been normalized to 1000. The last column gives the labels of experimentally inferred $2p^5 3s^2 3p^4$ levels (Table V).

	Calculation					Experiment	
Transition	n	J	E (eV)	I	ΔE (meV)	E (eV)	Label
$2p^4(^1D_2) \rightarrow 2p^5 3s^2 3p^4$	1	1/2	223.11	0.0	431		
	2	7/2	222.58	0.9	429		
	3	5/2	222.11	7.8	430		
	4	5/2	221.84	15.9	429	221.74	
	5	3/2	221.64	8.7	435		
	6	3/2	221.32	34.0	438	221.21	
	7	1/2	221.18	6.4	432		
	8	3/2	220.54	12.5	487		
	9	5/2	220.29	16.9	433	220.31	
	10	1/2	219.91	0.6	427		
	11	1/2	219.63	12.0	427		
	12	7/2	219.61	180.6	429	219.61	*A*
	13	3/2	219.48	18.4	512		
	14	3/2	218.71	14.0	651		
	15	5/2	217.90	149.2	462	217.87	*B*
	16	3/2	217.00	81.5	686	216.89	*C*
	17	5/2	216.32	225.6	707	216.22	*D*
	18	1/2	216.00	8.6	599		
	19	3/2	216.20	65.5	480	(215.67)	
	20	3/2	214.60	83.7	740	214.73	E'
	21	1/2	214.14	57.0	573	214.17	E''
$2p^4(^1D_2) \rightarrow 2p^5 3s^1 3p^5$	32	3/2	203.70	26.5	528		
	33	5/2	203.46	15.9	485		
	35	5/2	201.52	74.9	535	201.5	
	38	3/2	199.58	9.5	457	199.7	
$2p^4(^1D_2) \rightarrow 2p^5 3s^0 3p^6$	40	3/2	186.37	10.4	514		
	41	1/2	184.15	6.4	511		
$2p^4(^1S_0) \rightarrow 2p^5 3s^2 3p^4$	12	7/2	229.21	1.4	416		*A*
	13	3/2	229.08	4.2	499		
	15	5/2	227.50	1.2	449		*B*
	16	3/2	226.60	17.7	673	226.43	*C*
	17	5/2	225.92	0.2	694		*D*
	18	1/2	225.60	38.6	586	225.60	
	19	3/2	225.80	21.7	467		
	20	3/2	224.20	44.0	727	224.27	E'
	21	1/2	223.74	1.0	560		E''
	all others have intensities <1						
$2p^4(^1S_0) \rightarrow 2p^5 3s^1 3p^5$	39	1/2	208.47	9.0	491		

ergy of 2660.51(12) eV [20], this level is located at 545.75(32) eV above the neutral Ar ground state. The statistical weights suggest that most of the ions take the further decay route $2p^4(^1D_2) \rightarrow 2p^5 3s^2 3p^4 \rightarrow 3s^2 3p^2$. By addition of the first four ionization potentials the $Ar^{4+} 3s^2 3p^2(^3P_0)$ ground-state energy is obtained at 143.94 eV; the other $3p^2$ levels lie relatively to it at 0.0949 ($^3P_1$), 0.2519 ($^3P_2$), 2.0211 ($^1D_2$), and 4.7007 ($^1S_0$) eV [21]. This puts the total energy difference $\varepsilon = E(2p^4(^1D_2)) - E(3p^2)$ around 401 eV. Indeed three pairs of lines are found the sum energies of which agree within 0.02 eV and yield $\varepsilon = 400.69 \pm 0.09$ eV, in accordance with the value 400.6 ± 0.3 eV that has been determined likewise from the spectrum taken at somewhat lower resolution [4]. Three more line pairs support the same value of ε but can be localized only with a slightly lesser precision due to line overlap.

The experimentally determined value of ε does not fit with any of the values calculated from the $3p^2$ level energies quoted above. If we tentatively identify the final state of said pairs with $3p^2(^1D_2)$, more line pairs are expected with sum

TABLE IV. Transitions $2p^5(3s^23p^4+3s^13p^5+3s^03p^6)\rightarrow(3s^23p^2+3s^13p^3+3s^03p^4)$. Upper levels are enumerated as LM^2/n_i, $n_i=1,\ldots,41$ (Table I), lower ones as M^4/n_f, $n_f=1,\ldots,20$ (Table II). J_i is the total angular momentum of the upper level, Q_f the quantum symbol of the lower one. E denotes the energy, I the intensity (normalized as in Table III) and ΔE the width of the transition ($a[-n]$ stands for $a\times10^{-n}$). Capital letter labels refer to the experimentally inferred $2p^53s^23p^4$ levels (Table V).

	Calculation								Experiment
Transition	n_i	J_i	Label	n_f	Q_f	E (eV)	I	ΔE (eV)	E (eV)
$2p^53s^23p^4 \rightarrow 3s^23p^2$	12	7/2	A	5	$^1S_0$	178.40	25.3	6.51[-3]	178.42
	12	7/2	A	4	$^1D_2$	181.08	121.4	6.51[-3]	181.06
	6	3/2		3	$^3P_2$	181.14	7.3	1.55[-2]	
	6	3/2		2	$^3P_1$	181.29	9.3	1.55[-2]	
	6	3/2		1	$^3P_0$	181.39	0.1	1.55[-2]	
	18	1/2		5	$^1S_0$	182.01	7.3	1.76[-1]	181.99
	15	5/2	B	4	$^1D_2$	182.79	55.1	3.95[-2]	182.82
	13	3/2		3	$^3P_2$	182.98	6.9	8.90[-2]	
	13	3/2		2	$^3P_1$	183.13	5.6	8.90[-2]	
	13	3/2		1	$^3P_0$	183.23	1.6	8.90[-2]	
	20	3/2	E'	5	$^1S_0$	183.41	17.8	3.18[-1]	(183.45)
	16	3/2	C	4	$^1D_2$	183.69	34.4	2.63[-1]	
	21	1/2	E''	5	$^1S_0$	183.87	10.9	1.50[-1]	(183.86)
	17	5/2	D	4	$^1D_2$	184.37	82.3	2.84[-1]	184.49
	19	3/2		4	$^1D_2$	184.49	29.7	5.76[-2]	
	15	5/2	B	3	$^3P_2$	184.56	40.4	3.95[-2]	
	15	5/2	B	2	$^3P_1$	184.71	8.2	3.95[-2]	
	15	5/2	B	1	$^3P_0$	184.81	0.4	3.95[-2]	
	16	3/2	C	3	$^3P_2$	185.46	0.9	2.63[-1]	
	16	3/2	C	2	$^3P_1$	185.61	25.1	2.63[-1]	(185.57)
	16	3/2	C	1	$^3P_0$	185.71	0.4	2.63[-1]	
	20	3/2	E'	4	$^1D_2$	186.09	30.6	3.18[-1]	
	17	5/2	D	3	$^3P_2$	186.14	65.7	2.84[-1]	186.10
	17	5/2	D	2	$^3P_1$	186.29	12.9	2.84[-1]	
	19	3/2		2	$^3P_1$	186.41	18.5	5.76[-2]	
	18	1/2		3	$^3P_2$	186.46	5.0	1.76[-1]	
	19	3/2		1	$^3P_0$	186.51	8.8	5.76[-2]	
	21	1/2	E''	4	$^1D_2$	186.55	11.5	1.50[-1]	
	18	1/2		2	$^3P_1$	186.61	7.6	1.76[-1]	
	18	1/2		1	$^3P_0$	186.71	2.9	1.76[-1]	
	20	3/2	E'	3	$^3P_2$	187.86	34.5	3.18[-1]	187.90
	21	1/2	E''	3	$^3P_2$	188.32	5.7	1.50[-1]	
	21	1/2	E''	2	$^3P_1$	188.47	8.9	1.50[-1]	188.61
	21	1/2	E''	1	$^3P_0$	188.57	3.4	1.50[-1]	
$2p^53s^23p^4 \rightarrow 3s^13p^3$	17	5/2	D	13	$^1D_2$	167.27	12.0	2.84[-1]	
	15	5/2	B	9	$^3D_3$	169.71	26.7	3.95[-2]	
	20	3/2	E'	10	$^3P_2$	170.53	20.6	3.18[-1]	
	17	5/2	D	9	$^3D_3$	171.29	38.7	2.84[-1]	
$2p^53s^23p^4 \rightarrow 3s^03p^4$	12	7/2	A	19	$^1D_2$	149.26	21.6	6.51[-3]	149.1
$2p^53s^13p^5 \rightarrow 3s^13p^3$	35	5/2		13	$^1D_2$	182.07	9.2	1.13[-1]	181.99
	35	5/2		9	$^3D_3$	186.09	26.5	1.13[-1]	186.10
$2p^53s^13p^5 \rightarrow 3s^03p^4$	35	5/2		19	$^1D_2$	167.35	12.7	1.13[-1]	

energies shifted against ε by the precisely known energy differences $E(^1S_0)-E(^1D_2)$,$E(^3P_2)-E(^1D_2)$, etc. Within a tolerance of 0.1 eV 10 such pairs out of 12 possible have been found, while the alternative assumption that the pairs with $\varepsilon=400.69$ end up in one of the ^3P levels lead at most to four of the expected combinations. We therefore identify the level at $545.75-400.69=145.06\pm0.33$ eV with $3p^2(^1D_2)$, whereby also the other $3p^2$ levels are fixed. This identification is indirectly confirmed by the agreement of the observed line pattern with the one resulting from the relativ-

TABLE V. Labels and energies of intermediate $2p^5 3p^4$ levels inferred from the observed spectrum.

Level	Energy (eV)
A	326.13
B	327.88
C	328.89
D	329.54
E'	331.10
E''	331.62

istic calculations to be presented below. The $Ar^{4+}(^3P_0)$ ground state level in this way is located at 143.04 ± 0.33 eV above the neutral ground state. This value deviates by 0.9 eV from the sum of the first four ionization potentials (each with a quoted uncertainty on the order of 0.01 eV [21]) and thus reveals an inconsistency of the data involved in the comparison. Most likely the error has to be sought in the values of the Ar III and Ar IV ionization potentials.

From the manifolds of observed line pairs with a common intermediate $2p^5 3s^2 3p^4$ state the corresponding level energies can be inferred. Six such levels (or possibly closely spaced groups of levels) labeled A to E'' have been energetically located, which are listed in Table V. Their energies agree within 0.1 eV with those determined previously at lower spectral resolution [4], with the exception of the closely spaced E' and E'' levels. These replace the former level E, which already had been suspected of being split. The levels A to E'' correspond to the final ones of the strongest transitions; altogether the $2p^5 3s^2 3p^4$ configuration includes 21 different levels.

So far we have considered only transitions from the dominantly populated $2p^4(^1D_2)$ upper level. At an energy of 9.60 eV above the $2p^4(^1D_2)$ level lies the $2p^4(^1S_0)$ one which is accessed by 12% of the K-$L_{23}L_{23}$ transitions {the $2p^4(^3P)$ level is not accessible in LS coupling and actually very weakly populated [20]}. Indeed we observe two lines that are shifted by 9.54 eV against the transitions from the $2p^4(^1D_2)$ level to the $2p^5 3s^2 3p^4$ E' and C levels, respectively, and hence are identified as $2p^4(^1S_0) \rightarrow E'$ and $2p^4(^1S_0) \rightarrow C$. A third line lies 9.37 eV above the $2p^4(^1D_2) \rightarrow D$ one and thus slightly off the expected position of a possible $^1S_0 \rightarrow D$ transition. Energies of the observed transitions $2p^4(^1D_2, ^1S_0) \rightarrow 2p^5 3s^2 3p^4$ are quoted in Table III.

We can now compute the energies of all conceivable transitions from the six inferred intermediate $2p^5 3p^4$ levels A to E'' to the spectroscopically known final $3s^2 3p^2$ ones. The locations of $[M_{23}^2]$ lines expected in this way can be compared to line positions obtained from a fit of Gaussian peaks to the observed spectrum. If also diagram and $[M]$ spectator lines known from the electron impact excited L_{23}-MM spectrum measured by Werme, Bergmark, and Siegbahn [3] are taken into account, all observed peaks but one in the interval 178–190 eV can be explained, in some cases in several ways. Such agreement permits us to propose line assignments also for the $2p^5 3p^4 \rightarrow 3s^2 3p^2$ transitions [4]. These assignments, which are based entirely upon experimental data, are confirmed by the relativistic calculations to be reported below, with the sole modifications that the theoretical intensities rule out some energetically possible alternative interpretations and similarly in some cases reveal an error committed in determining the proper one(s) of the closely spaced final ^3P components. Such corrections are not too surprising, for slight distortions and shifts of some of the observed lines are likely to be present, because also the $2p^5 3s^1 3p^5 \rightarrow 3s^1 3p^3$ and other lines that are not included among the computed positions, are expected to fall into this energy range (cf. Fig. 2). Observed transition energies and assignments (modified according to the calculation) are given in Table IV.

By now we have successfully analyzed the observable spectrum in the region of the $L_{23}[L_{23}]$-$M_{23}M_{23}[L_{23}]$ and $L_{23}[M^2]$-$M_{23}M_{23}[M^2]$ transitions at the present level of resolution. Missing yet is a labeling of the inferred intermediate levels by quantum numbers. It would be unrealistic though to expect that these resolved levels—six out of actual 21 belonging to the $2p^5 3p^4$ configuration—can be identified solely by calculating *energies* at the presently achievable accuracy. Rather such calculations will have to be complemented by theoretical *transition probabilities*. Thereby one can also hope to assign additional, weaker lines, for which this could hardly be done in a credible way on a purely experimental basis, because they are intermixed with and overlapped by lines belonging to other partial spectra. The theoretical results reported in the next subsection will show that this is indeed possible.

C. $[L_{23}]$ and $[M^2]$ vacancy satellite spectra: Comparison of experiment and calculation

Energies and wavefunctions for the intermediate and final states of the Auger transitions have been obtained from multiconfiguration Dirac-Fock calculations as described in detail in Sec. III. Atomic states are represented in an intermediate coupling scheme so that only the total angular momentum J and the parity are finally conserved ''good'' quantum numbers for labeling the various levels. The expansion of the wave function was extended up to virtual single and double excitations into the $3d$ subshell (cf. Sec. III). A slightly simpler expansion basis was used to calculate also Auger transition rates and linewidths.

With such large expansions of the wave function we find a very good agreement of the results with experiment. For the transition multiplets $2p^4 \rightarrow 2p^5 3s^2 3p^4$ and $2p^4 \rightarrow 2p^5 3s^1 3p^5$, i.e., almost the entire $[L_{23}]$ spectrum, this is shown in Fig. 4. In this one and the following figures the theoretical spectrum of Lorentzian lines has been convolved with a Gaussian instrumental resolution function of 0.35 eV FWHM. Transitions with a calculated intensity exceeding 5% of the strongest line in the entire spectrum are in addition represented individually by appropriate Voigt profiles at the bottom of the figures. The transition multiplets ending, respectively, on the $2p^5 3s^2 3p^4$ and $2p^5 3s^1 3p^5$ levels appear well separated in energy. However, whereas the $2p^4 \rightarrow 2p^5 3s^0 3p^6$ doublets (outside the energy range of Fig. 4) and the $2p^4 \rightarrow 2p^5 3s^1 3p^5$ transitions are more or less buried under other lines, the strong $2p^4 \rightarrow 2p^5 3s^2 3p^4$ multiplet is almost free of contamination by other partial spectra (cf. Fig. 2). Especially here it is seen that the agreement between

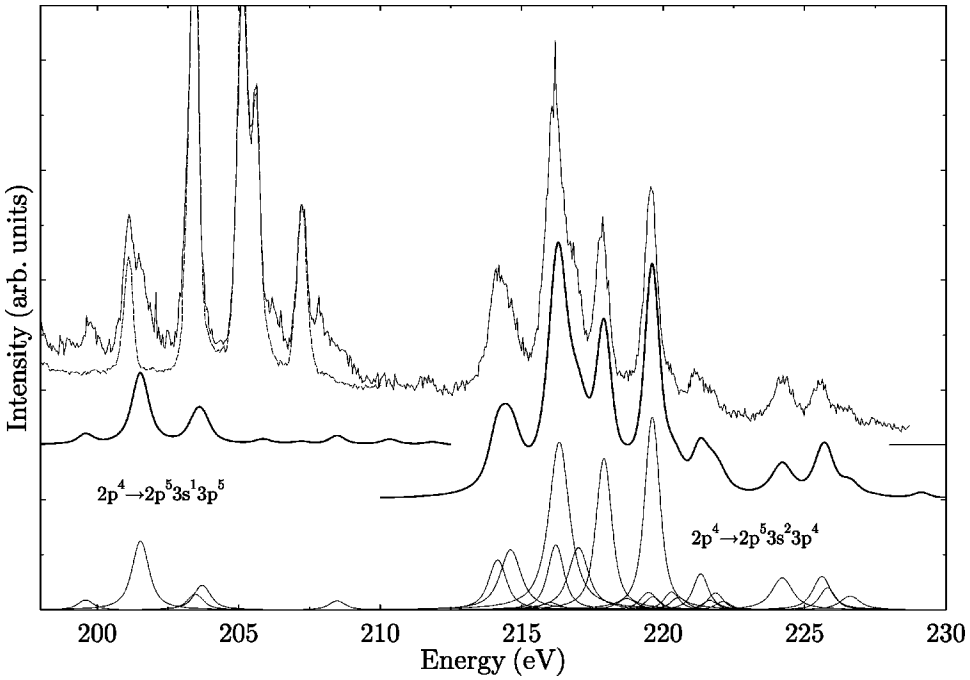

FIG. 4. Top of figure: observed photoexcited electron spectrum (continuous line) together with electron impact excited one (dotted). Heavy lines: calculated $L_{23}[L_{23}]$-$MM[L_{23}]$ transition multiplets (convolved by an instrumental Gaussian of 0.35 eV FWHM). The theoretical spectra have been suitably normalized to the experimental one. Bottom: calculated Auger lines exceeding 5% of the strongest one.

experiment and calculation is very close indeed, the deviation of the energies being below 0.2 eV wherever a precise comparison is possible. Since, on the other hand, the 21 $2p^4 \rightarrow 2p^5 3s^2 3p^4$ lines (18 of which have noticeable intensity) spread over 9 eV, some of them closely overlap each other, demonstrating how important for the analysis of the spectrum it is to know not only the theoretical transition energies but the probabilities as well.

Detailed results of the calculations for the more intense lines of the $2p^4 \rightarrow 2p^5(3s^2 3p^4 + 3s^1 3p^5 + 3s^0 3p^6)$ spectrum and a comparison with observed transition energies are presented in Table III. We denote the final levels by LM^2/n, $n=1,\ldots,41$, in ascending order of energy as calculated, for the sake of uniqueness, with a restricted expansion of the wave function (cf. Sec. III). The splittings of the transition multiplet have been obtained from the observed energy difference (9.60 eV) of the $2p^4\,{}^1D_2$ and ${}^1S_0$ levels [20] and from the calculated splittings of the final level multiplet. The absolute energy distance between the $2p^4$ and the $2p^5(3s^2 3p^4 + 3s^1 3p^5 + 3s^0 3p^6)$ multiplets has been found by shifting the latter one so as to bring the $2p^4({}^1D_2) \rightarrow LM^2/12$ transition into coincidence with the strong spectral line observed at 219.61 eV. Intensities have been calculated adopting the observed initial population of the $2p^4\,{}^1D_2$ and ${}^1S_0$ levels via K-$L_{23}L_{23}$ transitions in the ratio 87:12 [20]. Throughout the paper intensities are quoted in a common normalization, setting the total intensity of the $2p^4({}^1D_2) \rightarrow 2p^5 3s^2 3p^4$ multiplet to 1000. Finally, line widths have been derived by adding the calculated widths of the upper $2p^4$ levels (${}^1D_2$: 0.423 eV, ${}^1S_0$: 0.410 eV) to those of the lower $2p^5 3s^h 3p^{6-h}$ levels (which range between 3.8 meV and 0.32 eV, cf. Table I).

Subtracting the transition energies from the experimental energy of the $2p^4({}^1D_2)$ level (545.75 ± 0.32 eV, see above) we arrive at absolute energies of the $2p^5(3s^2 3p^4 + 3s^1 3p^5 + 3s^0 3p^6)$ levels. These are listed in Table I, along with the weights of the leading configurations in the expansion of the wave function. The states with an open $3s$ subshell exhibit large admixtures of virtual higher excited configurations. But also the $2p^5 3s^2 3p^4$ states, which are rather pure in this respect, can in most cases be adequately described only in intermediate coupling, as we expected considering the comparable magnitudes of the $2p^5$ and the $3p^4$ splittings [4]. Hence they appear heavily mixed when represented in a pure coupling scheme like $J_{2p}J_{3p}$ or LS coupling. In the former one of these representations frequently both J_{2p} subshell levels mix into the same total J state. Therefore the transitions generally do not come as doublets all having the same $2p$ fine-structure splitting. On the other hand, levels $LM^2/12$ and $LM^2/15$ crudely approximate a ${}^2F_{7/2,5/2}$ doublet in LS coupling.

Table III shows that, due to the good agreement between experimental and theoretical multiplet splittings, the observed lines leading to the six intermediate levels A to E'' can be identified with particular transitions, although in one case (D) two strong lines overlap. It is noteworthy that the five most intense lines of the $2p^4({}^1D_2) \rightarrow 2p^5 3s^2 3p^4$ multiplet end up in levels (A to E') in which the $3p$ electrons are coupled so as to form a ${}^1D$ subshell state. The three lines observed around 225 eV are seen to have been correctly assigned to $2p^4({}^1S_0) \rightarrow 2p^5 3s^2 3p^4$ transitions, although the dominant contribution to the one at 225.60 eV comes from the final level $LM^2/18$ rather than $LM^2/17(D)$. This explains the deviation, mentioned above, of the line position from that expected for the ${}^1S_0 \rightarrow LM^2/17(D)$ transition. In fact the transition $2p^4({}^1S_0) \rightarrow LM^2/17(D)$ is very weak, while its counterpart starting from the $2p^4({}^1D_2)$ upper level represents the strongest line of the entire spectrum. Generally

variations by more than two orders of magnitude are found in the intensity ratios between transitions from the upper $^1D_2$ and $^1S_0$ levels to the same final ones.

While the comparison between experiment and calculation is straightforward for the $2p^4 \rightarrow 2p^5 3s^2 3p^4$ multiplet, it is hampered for the $2p^4 \rightarrow 2p^5 3s^1 3p^5$ transitions by the fact that these lines are overlapped with other spectra, above all with the much more intense ones of the $2p^5 \rightarrow 3p^4$ diagram transitions. The contributions of these lines, which arise largely from primary L_{23} ionization, can be assessed with the aid of the electron impact excited $L_{23}-MM$ spectrum (dotted line in Fig. 4), which in the pertinent energy range consists of them exclusively. The difference between this spectrum and the photoexcited one is well compatible with the calculated $2p^4 \rightarrow 2p^5 3s^1 3p^5$ lines. Specifically, the line at 199.7 eV and the shoulder at 201.5 eV can be identified, respectively, with the transitions $2p^4(^1D_2) \rightarrow LM^2/n$, $n = 38$ and 35. On the other hand there are evidently contributions of a different origin, which presumably have to be attributed, together with some quasicontinuous background, to the $L_{23}[LM]$-$M_{23}M_{23}[LM]$ transitions (cf. Sec. IV A). Concluding the discussion of the $L_{23}[L_{23}]$-$MM[L_{23}]$ transitions, we can state that the calculation is in very good agreement with the observed spectrum, both with respect to transition energies as well as intensities, in those parts where there is little overlap with other partial spectra, and is at least well compatible with it in the others.

We now turn towards the spectrum emitted in the subsequent step of the deexcitation cascade, i.e. to the $L_{23}[MM]$-$MM[MM]$ lines. Calculations similar to those reported above have been performed also for the $2p^5(3s^2 3p^4 + 3s^1 3p^5 + 3s^0 3p^6) \rightarrow (3s^2 3p^2 + 3s^1 3p^3 + 3s^0 3p^4)$ transitions. The Auger energies have been obtained as the energy differences between the calculated upper levels (determined as described above including a small empirical shift of the entire multiplet) and the spectroscopically known lower ones [21] (referred to the Ar^{4+} ground level, which was located at 143.04 ± 0.33 eV as detailed in Sec. IV B). Thereby any possible errors of the theoretical $L_{23}[MM]$-$MM[MM]$ energy splittings hinge essentially on the calculated splittings of the upper level multiplet, while the distance between the upper and lower multiplets has been fitted to the observed Auger spectrum. Final levels not known spectroscopically have been obtained by calculation (cf. Sec. III). The energies of the $(3s^2 3p^2 + 3s^1 3p^3 + 3s^0 3p^4)$ levels are listed in Table II, together with the weights of the most important configurations in the expansion of the wavefunction. The levels are denoted by M^4/n, $n = 1, \ldots, 20$ in the order of ascending energy. Especially those with an empty $3s$ subshell exhibit strong correlation.

Line intensities have been computed from the theoretical populations of the upper $2p^5 3s^h 3p^{6-h}$ levels, as they result via transitions from the $2p^4(^1D_2, ^1S_0)$ levels, and from calculated rates of the subsequent transitions to the $3s^j 3p^{4-j}$ levels. The resulting spectrum and its partial multiplets, comprising altogether 820 transitions, are displayed in Figs. 5 and 6. Energies of all transitions stronger than 5% of the $2p^4(^1D_2) \rightarrow LM^2/12$ one are listed in Table IV and compared to observed line energies. We included in the table also some lines that exceed the 5% limit only by superposition. Intensities are given in a normalization common with the one

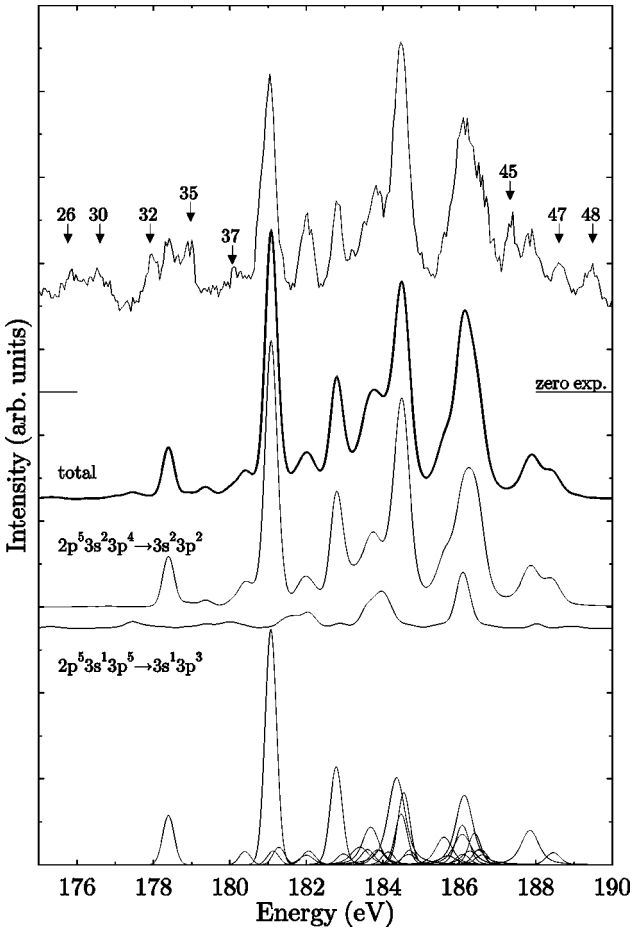

FIG. 5. Top: observed photoexcited electron spectrum with baseline (zero exp.). Arrows denote lines belonging to the normal (electron impact excited) L_{23}-MM spectrum with numbers according to Werme [3]. Middle: calculated $L_{23}[M^2]$-$M_{23}M_{23}[M^2]$ line multiplets and their sum (total), convolved by an instrumental Gaussian of 0.35 eV FWHM. Bottom: calculated Auger lines exceeding 5% of the strongest one. The relative normalization of experimental and calculated spectra is the same as in Fig. 4.

of the preceding transitions. The quoted linewidths are the calculated ones of the upper levels. Generally the experimental assignments of the more intense observed lines are confirmed by the calculation, with a few minor corrections regarding the dominant component of final ^3P levels. Again we note that strong transitions connect the $2p^5 3s^2 3p^4$ levels with final $3s^2 3p^2(^1D_2)$ ones if in LS coupling they can approximately be described by a $3p^4(^1D)$ subshell state.

Figure 5 compares the observed spectrum between 175 and 190 eV with the calculated $2p^5 3s^2 3p^4 \rightarrow 3s^2 3p^2$ and $2p^5 3s^1 3p^5 \rightarrow 3s^1 3p^3$ transitions. Lines that are known from the electron impact excited normal L_{23}-MM spectrum are marked by arrows and numbers according to Werme [3]. Incidentally, also the $2p^4(^1D_2) \rightarrow 2p^5 3s^0 3p^6$ transition doublet is hidden under the $2p^5 3s^2 3p^4 \rightarrow 3s^2 3p^2$ multiplet (see Table III). The calculation reproduces the remainder of the experimental spectrum very well regarding the splittings, and quite satisfactorily also with respect to the line intensities. One exception is the line observed at 181.99 eV which, even though comprising several transitions, has a significantly low theoretical strength. However, one should keep in mind that

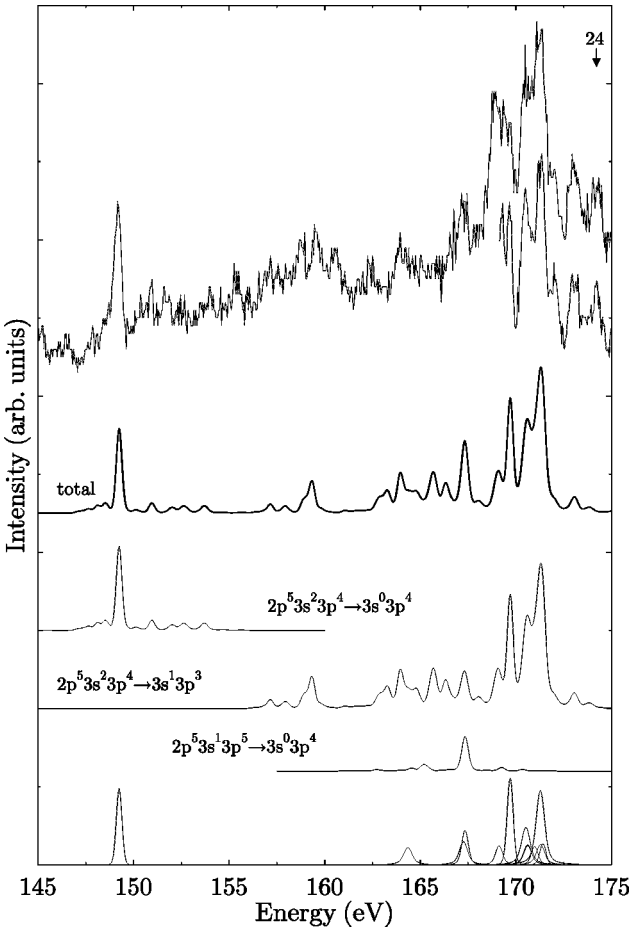

FIG. 6. Top: observed photoexcited electron spectrum (0.45 eV resolution [4]) and same with 0.35 eV resolution (169–175 eV). Middle: calculated $L_{23}[M^2]$-$MM[M^2]$ line multiplets and their sum (total), convolved by an instrumental Gaussian of 0.35 eV FWHM. Bottom: calculated Auger lines exceeding 5% of the strongest one. The relative normalization of experimental and calculated spectra is the same as in Fig. 4.

there exists a background contribution of spectra connected to higher final ionic charge states, which might be responsible for the discrepancy. The general good agreement of intensities would have been much inferior without due consideration of virtual $3d$ excitation in the calculation of transition probabilities. The quantitative importance of such virtual excitations is evident also from the comparatively high integrated strength of Auger transitions that have been observed below 160 eV in coincidence with final Ar^{4+} ions and have been attributed to correlation and shake satellites [7].

The remaining part of the $L_{23}[M^2]$-$MM[M^2]$ spectrum falls between 145 and 175 eV and is shown in Fig. 6. Here the observed spectra (unfortunately the better resolved one extends only down to 169 eV) exhibit in general broader features. From the electron-ion coincidence data (Fig. 2) we see that this energy range contains strong and even dominant contributions of other partial spectra. The prominent double peak structure near 170 eV arises in roughly equal parts from $L_{23}[M^2]$-$M_1M_{23}[M^2]$ and $L_{23}[M^3]$-$M_{23}M_{23}[M^3]$ transitions. Below 165 eV the e-ion coincidence signals from several ionic charge states are of comparable magnitude. Thus one has to expect a large number of lines that are alien to the $[M^2]$ spectrum. Statistically they appear to form a fairly smooth background though, for in spite of these contaminations one notes a surprisingly close correspondence between recognizable line structures in the observed and the theoretical $[M^2]$ spectrum. All fairly intense calculated peaks match well with measured ones. Most conspicuous is the isolated sharp line registered at 149.1 eV [$LM^2/12$ (A) $\rightarrow 3s^0 3p^4(^1D_2)$], which is excellently reproduced by theory in spite of the very strongly correlated nature of its final level. As is seen from the separate calculated lines at the bottom of Fig. 6, much overlap exists even in the $L_{23}[M^2]$ $-M_1M_{23}[M^2]$ spectrum itself.

Finally, let us come back to the extraction of the energy difference $\varepsilon = E(2p^4(^1D_2)) - E(3s^2 3p^2(^1D_2))$ from the experiment via identification of sequentially emitted pairs of lines (Sec. 4.2). The accuracy of ε (and hence the location of the Ar^{4+} ground level) might be impaired if the pertinent lines considerably overlap with others. The calculated spectrum shows that this is not the case and that indeed the lines at 219.61/181.06 and 217.87/182.82 eV are sufficiently isolated.

In conclusion, we have confirmed, refined and augmented here the analysis, given previously by von Busch *et al.* [4], of two new L_{23}-MM partial spectra, namely, the $L_{23}[L_{23}]$-$MM[L_{23}]$ and $L_{23}[M^2]$-$MM[M^2]$ transition multiplets. Relativistic multiconfiguration calculations of transition energies and intensities show such an excellent agreement with the observed spectrum that they—and only they—enabled us to extend the assignment to many additional weaker spectral lines. At the same time this success demonstrates that MCDF wave functions are well suited for the calculation of Auger spectra in cases with more than one open shell in the initial as well as several open shells in the final state. To our knowledge it is the first time that at least the strongest branch of the Auger cascade following deep-core ionization of an atom has been fully analyzed up to the present level of experimental resolution. In view of the enormous complexity of the L_{23}-MM cascade spectrum emitted after $1s$ ionization this success is due to favorable circumstances: the pertinent partial spectra are in their more important parts not much overlapped by other ones and contain a manageable number of sufficiently intense lines. Moreover the initial $2p^4$ and the final $3p^2$ and $3s^1 3p^3$ levels were known. In contrast, the weaker K-L_1L_{23} and K-L_1L_1 cascade branches involve L_1-$L_{23}M$ Coster-Kronig transitions, the final configurations of which ($L_{23}^{-2}M^{-1}$ or $L_{23}^{-2}M^{-2}$) split into a large number of levels that are still unknown. The intensity of the ensuing L_{23}-MM satellite spectra will be distributed over hundreds of lines, which are tedious to calculate and largely are not discernible in the quasicontinuous spectral background. Only around 170 eV a group of prominent lines appears which, according to the e-ion coincidence data, can at least in part be attributed to the $L_{23}[M^3]$-$M_{23}M_{23}[M^3]$ transitions [7]. But the analysis via sum energies of line pairs is not applicable here for lack of auxiliary data. Instead, e-ion or e-e coincidence experiments at high resolution might help to further advance the investigation of this extremely complex spectrum.

V. SUMMARY

The L_{23}-MM Auger spectrum emitted after $1s$ ionization of argon, although representing the simplest case yet of a

rare gas Auger cascade spectrum, contains hundreds, if not thousands of overlapping lines and therefore is difficult to investigate in detail. In fact it consists of at least eight complete L_{23}-MM spectra each emitted in the presence of a different configuration of spectator vacancies. The gross intensity distribution of these partial spectra—a prerequisite of a more detailed line analysis—has been determined previously. We have excited the L_{23}-MM cascade spectrum with broadband x rays and remeasured it at 0.35 eV resolution. By comparison with the electron impact excited L_{23}-MM spectrum a number of observed lines can be identified with known ones belonging to the L_{23}-MM and $L_{23}M$-MMM partial spectra. Most of the other more intense lines, however, arise from the strongest branch of K hole deexcitation which, after an initial K-$L_{23}L_{23}$ step, gives rise to consecutive emission of the $L_{23}[L_{23}]$-$MM[L_{23}]$ and $L_{23}[M^2]$-$MM[M^2]$ spectra. Pairs of sequentially emitted lines have been identified and six intermediate $2p^5 3p^4$ levels energetically located. These results are compared to carefully optimized MCDF calculations of energies as well as transition probabilities for the entire $2p^4(^1D_2, ^1S_0) \rightarrow 2p^5(3s^2 3p^4 + 3s^1 3p^5 + 3s^0 3p^6)$ group of transitions, i.e., the $L_{23}[L_{23}]$-$MM[L_{23}]$ spectrum. Very good agreement is found between theory and experiment. This shows that the calculated splittings of the $2p^5 3s^k 3p^{6-k}$ levels can be considered reliable within 0.2 eV, and enables the assignment of quantum labels to the observed $2p^5 3p^4$ levels. By similar calculations also the experimental identification of the subsequent $2p^5 3p^4 \rightarrow 3p^2$ transitions is confirmed. The calculations prove, however, even more powerful insofar as with their help a considerable number of additional, weaker $L_{23}[M^2]$-$MM[M^2]$ lines can be assigned. Thus it has been possible to fully analyze the two strongest partial spectra arising after $1s$ ionization practically to the limits of the present experimental resolution (0.35 eV). The remaining partial spectra consist of a large number of strongly overlapping and in general fairly weak lines so that a similar analysis appears not feasible.

ACKNOWLEDGMENTS

We are indebted to F. A. Parpia, I. P. Grant, and C. Froese Fischer for making available to us their unpublished MCDF code GRASP[2]. Thanks are due to Detlef Reich who generated several figures. This work was funded by the German Federal Minister for Research and Technology (BMFT) under Contract No. 05 5PDAXI 8. S.F. acknowledges support by the Deutsche Forschungsgemeinschaft (DFG) in the framework of the Schwerpunkt ''Wechselwirkung von Laserfeldern mit Materie.''

[1] W. Mehlhorn and D. Stalherm, Z. Phys. **217**, 294 (1968).
[2] L. O. Werme, T. Bergmark, and K. Siegbahn, Phys. Scr. **6**, 141 (1972).
[3] L. O. Werme, T. Bergmark, and K. Siegbahn, Phys. Scr. **8**, 149 (1973).
[4] F. von Busch, J. Doppelfeld, C. Günther, and E. Hartmann, J. Phys. B **27**, 2151 (1994).
[5] M. H. Chen, B. Crasemann, and H. Mark, At. Data Nucl. Data Tables **24**, 13 (1979).
[6] U. Arp, T. LeBrun, S. H. Southworth, M. A. MacDonald, and M. Jung, Phys. Rev. A **55**, 4273 (1997).
[7] U. Alkemper, J. Doppelfeld, and F. von Busch, Phys. Rev. A **56**, 2741 (1997).
[8] C. Günther and E. Hartmann, Nucl. Instrum. Methods Phys. Res. B **98**, 74 (1995).
[9] J. Doppelfeld, Doctoral thesis, University of Bonn, Germany (unpublished).
[10] E. J. McGuire, Phys. Rev. A **11**, 1880 (1975).
[11] K. G. Dyall and F. P. Larkins, J. Phys. B **15**, 2793 (1982).
[12] T. Åberg and G. Howat, in *Handbuch der Physik*, edited by W. Mehlhorn (Springer, Berlin 1982), Vol. 31, p. 469.
[13] I. P. Grant, in *Methods in Computational Chemistry*, edited by S. Wilson (Plenum Press, New York, 1988), Vol. 2, p. 1.
[14] I. P. Grant, B. J. McKenzie, P. H. Norrington, D. F. Mayers, and N. C. Pyper, Comput. Phys. Commun. **21**, 207 (1980).
[15] F. A. Parpia, I. P. Grant, and C. Froese Fischer (unpublished); F. A. Parpia, C. Froese Fischer, and I. P. Grant, Comput. Phys. Commun. **94**, 249 (1996).
[16] S. Fritzsche, Doctoral thesis, University of Kassel, Germany, 1992 (unpublished).
[17] S. Fritzsche and B. Fricke, Phys. Scr. **T41**, 45 (1992).
[18] S. Fritzsche, B. Fricke, and W.-D. Sepp, Phys. Rev. A **45**, 1465 (1992).
[19] W. Ong and A. Russek, Phys. Rev. A **17**, 120 (1978).
[20] L. Asplund, P. Kelfve, B. Blomster, H. Siegbahn, and K. Siegbahn, Phys. Scr. **16**, 268 (1977).
[21] S. Bashkin and J. O. Stoner Jr., *Atomic Energy-Levels and Grotrian Diagrams* (North-Holland, Amsterdam, 1978).
[22] K. G. Dyall, I. P. Grant, C. T. Thomson, F. A. Parpia, and E. P. Plummer, Comput. Phys. Commun. **55**, 425 (1989).
[23] J. Hansen and W. Persson, J. Phys. B **20**, 693 (1987).
[24] J. W. Cooper, S. H. Southworth, M. A. MacDonald, and T. LeBrun, Phys. Rev. A **50**, 405 (1994).
[25] M. Breinig, M. H. Chen, G. E. Ice, F. Parente, B. Crasemann, and G. S. Brown, Phys. Rev. A **22**, 520 (1980).